



HAL
open science

Nanoindentation characterization of the surface mechanical properties of a 17-4PH stainless steel substrate treated with grit blasting and coated with a Cr₃C₂-NiCr coating

J.-B. Giouse, K. White, C. Tromas

► To cite this version:

J.-B. Giouse, K. White, C. Tromas. Nanoindentation characterization of the surface mechanical properties of a 17-4PH stainless steel substrate treated with grit blasting and coated with a Cr₃C₂-NiCr coating. *Surface and Coatings Technology*, 2019, 368, pp.119-125. 10.1016/j.surfcoat.2019.01.050 . hal-02284915

HAL Id: hal-02284915

<https://hal.science/hal-02284915>

Submitted on 22 Oct 2021

HAL is a multi-disciplinary open access archive for the deposit and dissemination of scientific research documents, whether they are published or not. The documents may come from teaching and research institutions in France or abroad, or from public or private research centers.

L'archive ouverte pluridisciplinaire **HAL**, est destinée au dépôt et à la diffusion de documents scientifiques de niveau recherche, publiés ou non, émanant des établissements d'enseignement et de recherche français ou étrangers, des laboratoires publics ou privés.



Distributed under a Creative Commons Attribution - NonCommercial 4.0 International License

Nanoindentation characterization of the surface mechanical properties of a 17-4PH stainless steel substrate treated with grit blasting and coated with a Cr₃C₂-NiCr coating

J.-B. Giouse^{1,2}, K. White¹, C. Tromas²

¹*Department of mechanical engineering at the University of Houston*

²*Institut Pprime, UPR 3346 CNRS - Université de Poitiers – ENSMA*

Keywords: *nanoindentation cartography; 17-4PH steel substrate; surface treatment; cermet coating; ceramic/metal interface; high velocity oxy fuel (HVOF) spraying*

Abstract

Grit blasting with alumina particles offers a conventional substrate surface preparation method intended to improve the adhesion of thermal spray coatings. However, the associated microstructural modifications to the substrate may, in fact, reduce the integrity of the interface. In this paper, we use nanoindentation cartography methods to characterize the local mechanical properties of the interface of a HVOF coating deposited on an alumina grit blasted 17-4PH stainless steel substrate. The results show a hardness gradient in the substrate, which we evaluate within the context of the refinement of the substrate microstructure. We show that nanohardness mapping, combined with Atomic Force Microscopy and Scanning Electron Microscopy analysis provides a viable approach to study this unique contribution of the microstructural relationship between the beneficial and detrimental impacts of grit blasting on the adhesion of thermal spray coatings.

I. INTRODUCTION

Thermal spray coatings are commonly used in many industrial applications including the automobile, petroleum or civil engineering industries. High Velocity Oxy-Fuel (HVOF) spraying is specifically useful for extreme applications like the deposition of cermet materials that requires high velocities to be deposited. Thermal spray coatings deposited by HVOF can enhance the surface properties of a material such as wear and corrosion resistance [1], [2]. Prior to deposition of the coating, substrate surface modification treatments, such as grit

blasting may optimize the local roughness (**Figure 1**) to favor the mechanical interlocking of the coating [3]–[5]. This common surface treatment sends high velocity particles (usually angular shaped alumina or silicon carbide grit) onto the substrate surface in order to cause impact damage.

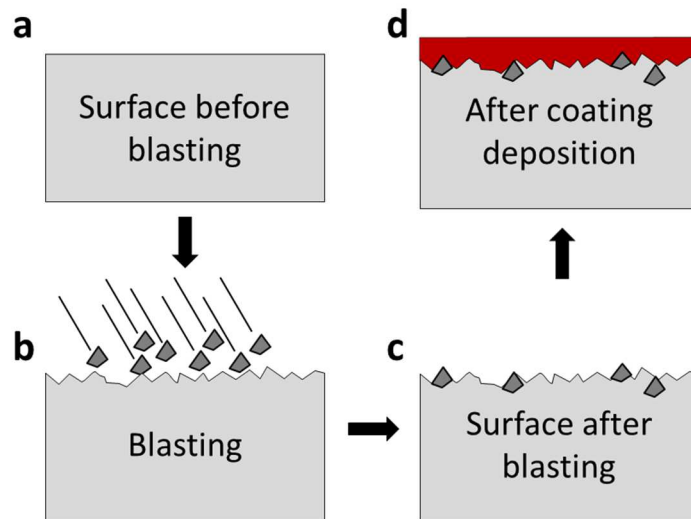


Figure 1. Simplified steps occurring during a grit blasting process. The particles are blasted onto the substrate surface to increase the roughness and favor the mechanical interlocking of the coating particles. Some alumina particles remains embedded in the substrate after the process.

Reports shows opposing effect of the grit blasting on the fatigue properties. On one hand, some studies demonstrate a detrimental effect of grit blasting treatments on the fatigue lifetime, where the presence of embedded or adhered residual particles coupled with a high surface roughness can lead to important stress concentrations and a decrease of the fatigue performances [6], [7]. Cracks in the vicinity of the embedded particles were also observed in a 316 stainless steel subjected to waterjet peening [8] which highlight the stress concentration role of such defects. In addition, the high kinetic energy associated with the process creates a complex microstructural and stress state in the subsurface, further modifying the fatigue and mechanical properties of the treated material [7], [9]–[11]. On the other hand, it was also reported that the detrimental impact on the fatigue properties induced by the modification of the roughness and the embedded particles can sometimes be compensated and even inversed when sufficient compressive stresses are generated. Thus, several studies actually

reported an increase of the fatigue properties due to the positive impact of the compressive stresses on the crack nucleation [12].

Nevertheless, in the case of grit blasting used before the deposition of a coating, those defects associated with the grit blasting process have numerous effects on adhesion. First, the modification of the microstructure and stress state can modify how the splats behave when impinging the substrate. Gao and al. [13] conducted a study on the influence of hardness on the deposition of single coating splats, showing that sufficient deformation of the substrate is necessary to promote adhesion. Moreover, the presence of adhered residual grits on the substrate surface locally degrades the adhesion of the coating by modifying the wetting properties of coating particles and by blocking any interactions between the coating and the substrate.

In this paper, we propose a new methodology to characterize the impact of grit blasting on a 17-4PH steel substrate coated with a cermet $\text{Cr}_3\text{C}_2\text{-NiCr}$ coating. To achieve this, the nanoindentation cartography method was used in cross section, in which the hardness data links the microstructural modifications induced by the grit blasting to the resulting local substrate mechanical properties in the vicinity of the interface. The nanoindentation measurements are coupled to atomic force microscopy (AFM) and scanning electron microscopy (SEM) observations.

II. MATERIALS AND EXPERIMENT DETAILS

a. Materials and surface preparation

The substrate is a 17-4 precipitation hardening (17-4PH) martensitic steel. It is in the H1150 condition meaning that it underwent a heat treatment at 621°C from the solution treated condition. The surface of the steel substrate was prepared in two different ways prior the coating deposition process. One sample was grit blasted with alumina particles and another one was polished up to $1\mu\text{m}$ with diamond suspension.

Following the surface treatments, both samples were coated with a cermet material made of chromium carbides Cr_3C_2 embedded in a NiCr metallic binder (80% Cr_3C_2 - 20% NiCr). The coating is produced by high velocity oxy fuel (HVOF) spraying and is 250 μm thick.

Samples were cut and embedded in a carbon filled resin using a hot mounting press as shown in **Figure 2**. Preparation of the cross section involves conventional metallographic preparation followed by chemical mechanical polishing (CMP) using non-crystallizing colloidal silica in order to achieve a minimum roughness and no work hardening of the surface. Thus, the mechanical properties measured by nanoindentation are not altered by the surface condition.

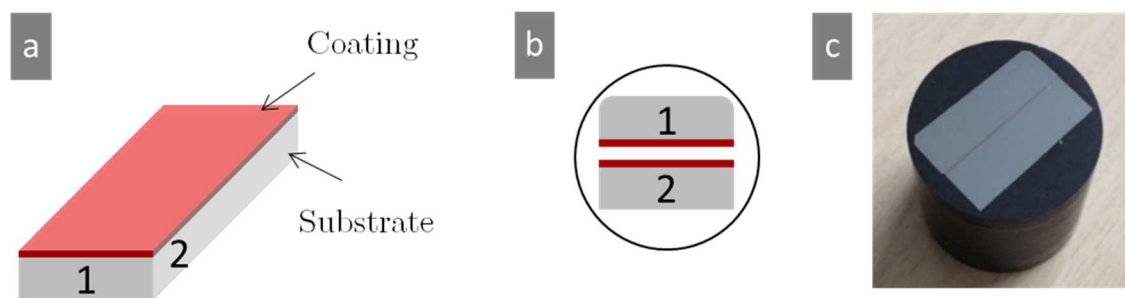


Figure 2. Preparation steps of the samples. Each sample is cut from a bar and mounted into a conductive carbon resin. (a) Schematic of the coated bar as received by the manufacturer. The coating is in red and the substrate in grey. (b) Schematic representation of the samples as mounted in the resin. Two samples were used and faced each other to favor a uniform polishing. (c) Photograph of the samples mounted in a conductive carbon filled resin.

b. Analysis techniques

Microstructural observations were performed by scanning electron microscopy using a JEOL JSM-7001F. The SEM was used both in secondary (SE) and back scattered electrons (BSE).

Atomic force microscopy was carried out using a Dimension 3100 microscope from Bruker (Santa Barbara, CA) in tapping mode in order to characterize the surface resulting from the sample preparation. The AFM files were processed using the WSxM software [14].

c. Nanoindentation

A U-NHT nanoindenter from Anton Paar (Peseux, Switzerland) equipped with a Berkovich tip was used to perform the nanoindentation measurements. This apparatus has an active surface reference ensuring very high thermal and mechanical stabilities. The tip was carefully calibrated using the regular method, consisting of indenting a material with a known Young's modulus, in this case fused silica ($E=72\text{GPa}$). The hardness was determined by analyzing the elastic unloading curve using the effective indenter method [15], [16].

In order to characterize the local mechanical response, the nanoindentation cartography method has been applied. This method consists in performing a regular matrix of indents in order to reconstruct a hardness map [17]–[19]. The nanoindentation cartography method allows the investigation of the local mechanical properties in heterogeneous materials and the correlation of the hardness variations with the chemical or microstructural heterogeneities of the material.

Figure 3a illustrates the loading sequence used during the nanoindentation tests in this work. The loading is performed in depth control to ensure that each indentation have the same maximum penetration depth, without regard to hardness. The unloading is performed in load control at $4000\mu\text{N}/\text{min}$. **Figure 3b** presents a typical nanoindentation curve obtained in cross section in the 17-4PH steel using the loading profile shown **Figure 3a**.

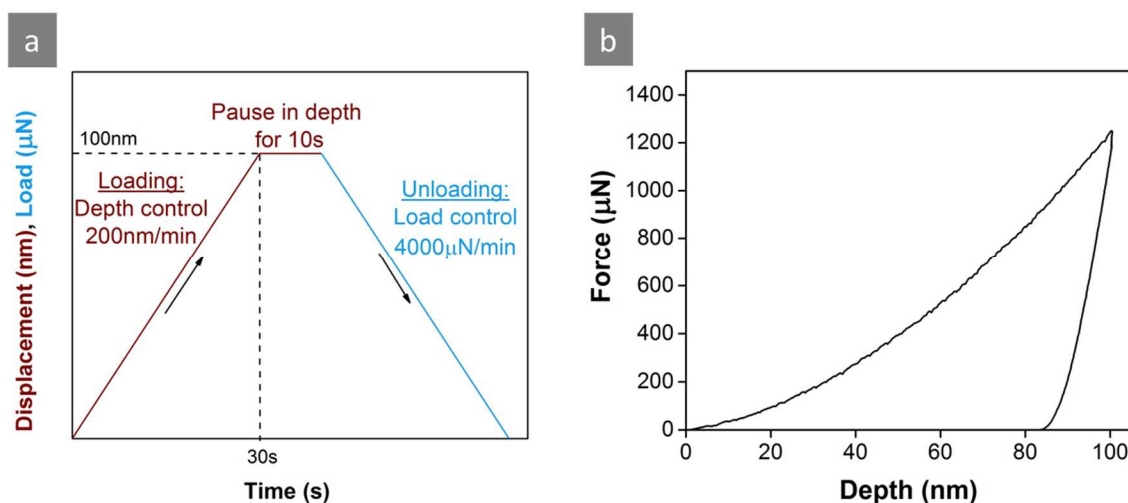


Figure 3. (a) Indentation profile. The loading is depth controlled to assure a constant penetration of all the indentations while the unloading is load controlled (b) Typical nanoindentation curve obtained in cross section in the 17-4PH steel using the loading profile shown Figure 3a.

For the cartography, the array was designed with a maximum indentation depth of 100nm and a distance between adjacent imprints of 3 μ m. These parameters were selected to minimize the step size of the array, and thus increase the resolution of the cartography, while ruling out the influence of the surface morphology. In the case of a Berkovich indenter, the diameter of an imprint is about 7 times its depth and it is common to use a minimum distance of 5 times the diameter, i.e. about 35 times the maximum indentation depth between two successive indentations.

A color chart has been associated with the hardness values, and a bicubic interpolation has been applied to build the map from the discrete dataset. Such an interpolation method was chosen as it leads to smoother images with fewer interpolation artifacts than either the nearest neighbor or the bilinear interpolations [19].

III. RESULTS AND DISCUSSION

a. Microstructure analysis

Figure 4 summarizes the results of the microstructural characterization of the interface. An optical micrograph of the interface, shown in **Figure 4a**, identifies the presence of two residual alumina particles from the grit blasting. **Figure 4b** is a zoomed image of the interface taken with the SEM. The average diameter of the particles is 20 μ m. Fully embedded particles were also observed, as shown later. When trapped, the particles modify the wetting properties of the coating particles during the deposition and impede the interaction between the coating and the substrate resulting locally in poorly bonded regions [20], [21]. Embedded alumina particles originate from important deformation of the substrate overlaying the particles during the process. It is usually associated with a complex surrounding stress state that can lead ultimately to failure [6], [22], [23]. The SEM image in **Figure 4b** reveals that the process also affects the microstructure of the substrate. Two microstructurally dissimilar regions can be distinguished inside the substrate. The region just beneath the interface is associated with an ultrafine-grained microstructure and is about 10-20 μ m. The rest of the substrate is

characterized by a grain size gradient up to the point where the process does not affect the microstructure anymore and the common lath martensitic structure is observed.

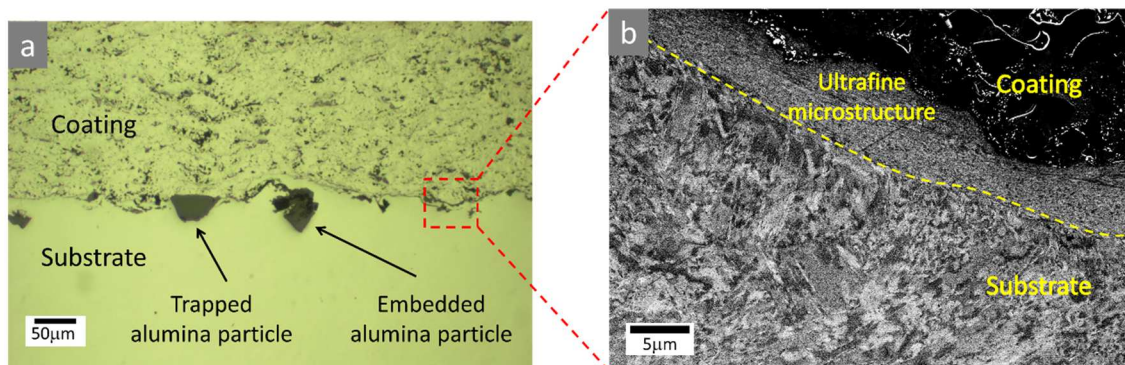


Figure 4. (a) Optical microscopy image of the coating/substrate interface showing adhered and embedded alumina particles. (b) SEM image of the interface in cross section revealing a change of microstructure of the substrate when approaching the interface.

Atomic force microscopy was used to inspect the surface after metallographic and chemical mechanical polishing (CMP) preparation and the results are shown **Figure 5**. **Figure 5b** is the 3D representation of the picture shown in **5a**. The line represents the position of the height profile shown in **5c**, which shows that the coating is standing 150nm above the substrate, resulting from different polishing rate during sample preparation. The slope of the profile extends over 12 μm corresponding to a slope of approximately 0.01°. A Root Mean Square (RMS) roughness of about 4nm was achieved in the 17-4 PH substrate. Both the slope and the roughness are sufficient for the nanoindentation measurements.

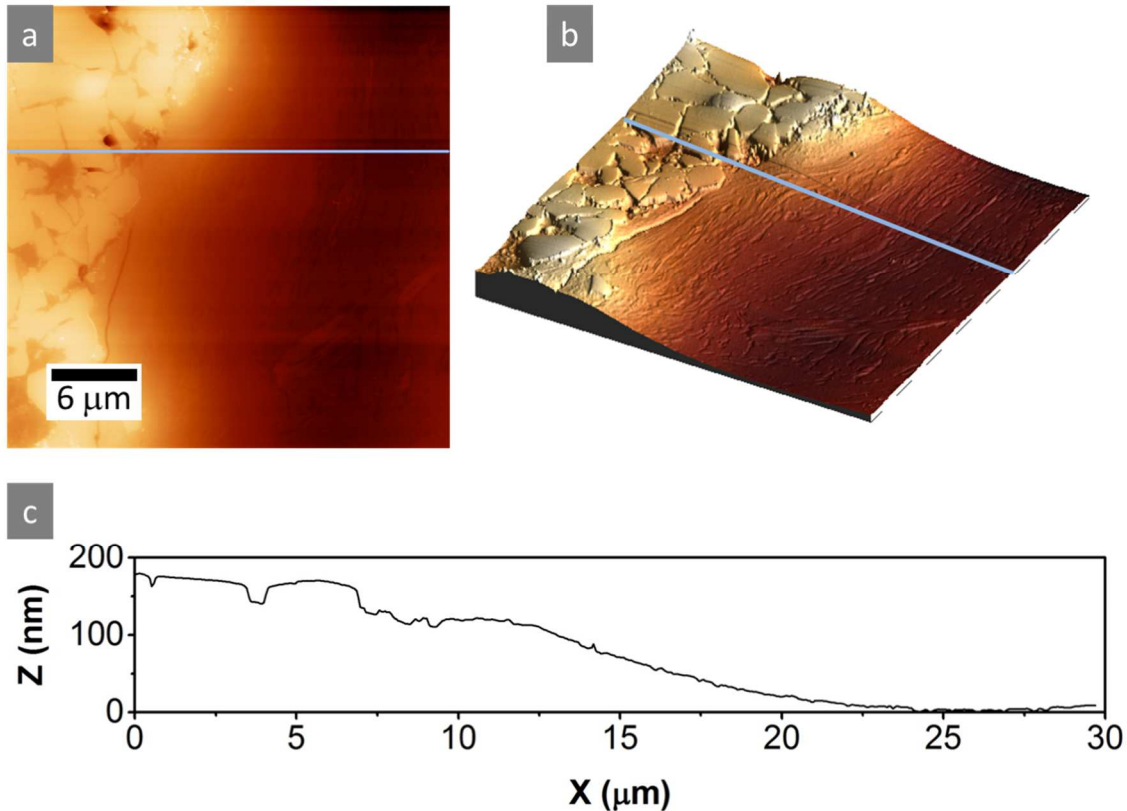


Figure 5. Data obtained from atomic force microscopy. (a) Topography image of the surface at the interface after CMP with colloidal silica. The blue line represents the position of the profile shown in Figure 5c. (b) 3D representation of the topography image shown in (a). The difference in depth between the substrate and the coating is clearly observable. The reader is referred to the profile shown in (c) for Z scale. (c) Height profile taken at the interface. Both the substrate and coating are flat. The slope corresponds to the near interface region of the substrate affected by the grit blasting and resulting from differential polishing rate during CMP.

b. Cartography

Figure 6 shows the hardness cartography determined from an array of 765 indents. The step size between each indentation is $3\mu\text{m}$. For a better analysis, the color scale has been adjusted to the substrate hardness values (the coating hardness values have been saturated and appear in grey contrast). The substrate presents a hardness gradient ranging from 4700MPa at $100\mu\text{m}$ away from the interface up to 5800MPa at the interface. The Young's Modulus was also measured and remains constant throughout the substrate thickness at $219 \pm 12\text{GPa}$. A similar value of 225GPa using the same method was found [24], thereby validating the hardness nanoindentation measurements. Moreover, the use of displacement control ensured that all indentations have the same size so that artefacts associated with any possible tip calibration uncertainties or with indentation size effect are averted.

A strong increase of the hardness is observed with a gradient of about $11\text{MPa}/\mu\text{m}$ and a hardness reaching a maximum of 5800MPa close to the interface. This hardness increase can have several consequences on the adhesion of the coating. First, it is likely to promote brittleness and modify the surface fatigue properties of the substrate. Furthermore, it can affect the coating build-up during the early stage of deposition. Indeed, research conducted by Gao et al. [13] revealed that a higher hardness of the substrate is associated with more particles rebounding from the substrate surface during the first stage of deposition.

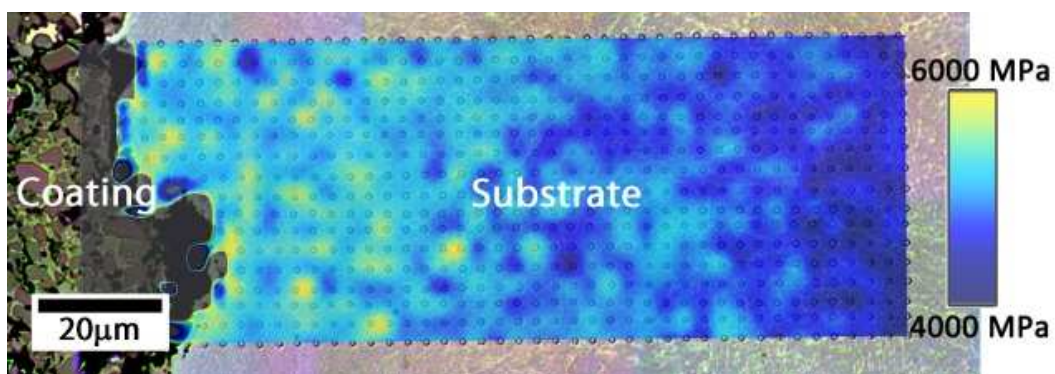


Figure 6. Nanohardness cartography built from a 17×45 nanoindentation array at the interface between the coating and the substrate. The hardness map is superimposed to the optical microscopy image of the indented area. The substrate surface was grit blasted with alumina particles prior to the deposition of the coating. The coating is on the left side and was voluntarily saturated to increase the contrast for the representation of hardness in the substrate.

Figure 7 shows the hardness cartography of the non-grit blasted substrate determined from 450 indents. The nanohardness remains constant throughout the substrate thickness at approximately 4700MPa .

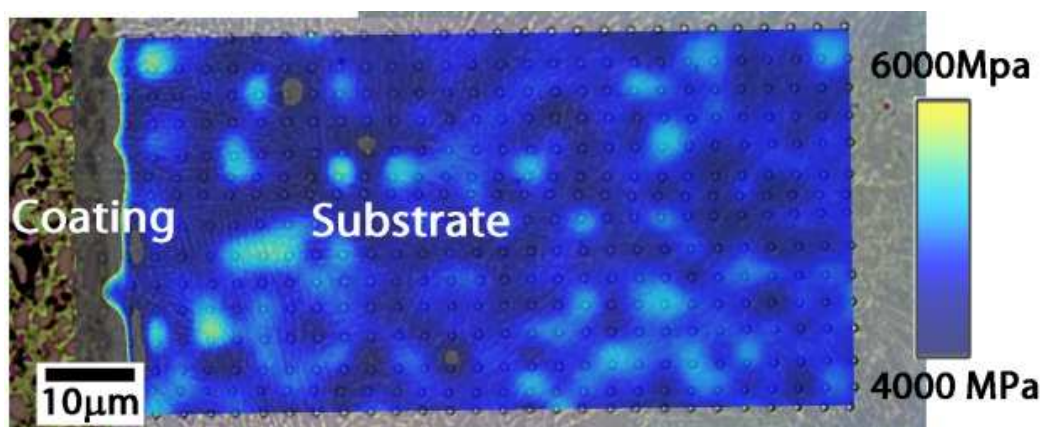


Figure 7. Nanohardness cartography built from a 15×30 nanoindentation array at the interface between the coating and the substrate. The hardness map is superimposed to the optical microscopy image of

the indented area. The substrate was polished with a diamond solution up to 1 μm prior to the deposition of the coating. No hardening is observed in the substrate.

The non-grit blasted sample exhibits no evidence of hardness gradient in the substrate. Comparison with cartography of the grit blasted sample shown **Figure 6** suggests that the grit blasting modifies the mechanical properties and increases the hardness. It also suggests that the coating deposition, despite high kinetic energy involved, does not induce any visible changes of the mechanical properties of the substrate. Yet, one would have expected some hardening due to the impact of the carbides contained in the coating. Thus, the contribution of the NiCr metallic phase in absorbing the deformation is probably non-negligible.

The impact of the grit blasting process on the microstructure was investigated by imaging the microstructure of the substrate at different distance from the interface. **Figure 8b** was taken in the bulk where the substrate has not been affected by the grit blasting process. The microstructure is a regular lath microstructure characteristic of martensitic steels [25]. **Figure 8a** was taken in the substrate, a few microns away of the interface, where the substrate is highly affected by the grit blasting process. The lath microstructure disappeared, replaced by a finer-grained structure.

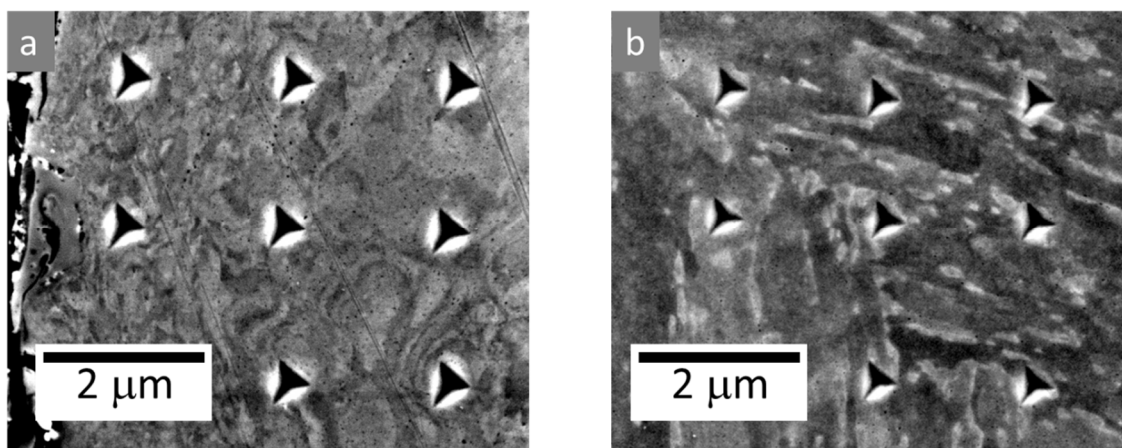


Figure 8. Electronic microscopy images revealing the microstructure of the substrate taken a) away of the interface b) at the interface. The microstructure at the interface is made of very small grains associated with deformation patterns while the microstructure in the bulk shows a regular lath microstructure.

The comparison of the microstructure shown in **Figure 8a** and **b** suggest that the high values of hardness measured at the interface is related to grain refinement induced by the grit

blasting process. Several papers have reported a change of microstructure when blasting high velocity particles on a metallic surface. The mechanisms of refinement are similar to the ones observed in severe plastic deformation processes such as high-energy shot peening or surface mechanical attrition treatment [26]–[28]. The plastic strains induced by the impacting particles are accommodated by a change of microstructure through dislocation motion and grain subdivision [29]. A gradient of microstructure and mechanical properties is usually observed in the impacted material because of the gradient of strain and strain rate induced.

c. Indentation size effect

The nanoindentation cartography has been performed at a low penetration depth (100nm) in order to reduce the matrix step size and thus to increase the spatial resolution. However, one may wonder if the hardness values depend on the penetration depth (ISE). For this reason, the effect of the penetration depth on the hardness measurement was investigated.

Indentation size effect (ISE) describes the scale dependence observed in various materials for which the hardness increases with decreasing the indentation size. In order to characterize a potential ISE in the substrate, fifteen rows of indents were made containing 15 indentations each for a total of 225 indentations. Each row corresponds to a different maximum penetration depth ranging between 80 and 700nm. The indentations were made in the bulk where the microstructure and hardness are considered homogeneous. The results of the ISE characterization are presented **Figure 9**. Each data point is an average of 15 hardness values. The hardness remains constant throughout the range, which indicates that there is no scale-dependence in the hardness values. The uncertainties at small penetration depths remain acceptable, which further validates the indentation procedure shown in **Figure 3a**.

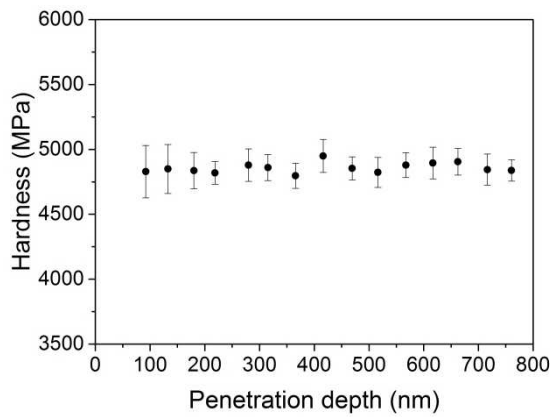


Figure 9. Nanohardness as a function of the penetration depth for ISE investigation. Each data point is the average of 15 hardness values obtained from indentations made at the same depth for a total of 225 indentations. The errors bars correspond to the standard deviation calculated from those 15 values. The hardness is constant throughout the entire range, which means no evidence of scale dependence in the hardness measurements is observed.

d. Embedded alumina particle

Grit blasting leaves residual particles on the substrate surface, which can adhere to the substrate or completely embed into the substrate surface. **Figure 10** illustrates the steps in performing and analyzing the cartography from a 12*15 indentations array around an alumina particle. The SEM image (**Figure 10a**) of the indented area taken using back scattered electrons, using a step size of 2 μ m provided increased resolution of this ultra-fine-grained microstructure. The yellow dash line separates this microstructure from the rest of the material. The diameter of the affected region is about 2-3 μ m. Small cracks nucleating from the particle (see red arrows on **Figure 10a**) and propagating into the substrate are clearly observable. An AFM image of the particle is shown **Figure 10b**. It shows deformation patterns on the surface, which follows the ultra-fine-grained microstructure observed in **Figure 10a**. In addition, the high resolution AFM resolves surface features for correlation with the hardness cartography shown in **Figure 10c**. A nearest neighbor interpolation method was used to reconstruct the hardness map. **Figure 10c** suggests that the hardness is notably higher in the vicinity of the particle. However, the hardness variations apply over very short distances, which make it difficult to extract clear information from the hardness map. To address this issue, one could think of increasing the resolution of the cartography by decreasing the step size of the array but further decreasing the step size would induce interactions between neighboring

indentations. One solution is then to look at the individual hardness values as shown in **Figure 10c**. The hardness values of the ultra-fine-grained region (delimited by the yellow dashed line) are ranging from 6.2 to 7.3GPa. Outside this region, the hardness ranges between 5.1 and 5.9GPa.

The SEM and AFM observations suggest that the vicinity of embedded alumina particles is severely altered and the mechanisms of refinement described earlier take place to a greater extent. It is commonly thought that the coating/substrate interface is the preferential path for failure. However, the presence of cracks around the embedded particles (red arrows in **Figure 10a**) indicates that the particles act as stress raisers and are preferential sites for crack nucleation. Additionally, we can also observe that those cracks propagate in the substrate, in the layer of affected microstructure, which suggests that the coating/substrate interface is not necessarily where the failure will occur. It is confirmed by the nanohardness cartography results, which indicate that the area surrounding the particles has higher hardness, which is likely to promote brittleness and thus crack propagation. **Figure 11** further illustrates the crack propagation in the substrate at different locations of the substrate/coating interface. In all optical images, a crack has nucleated from an alumina particle and has propagated through the substrate.

The results of the nanoindentation cartography and the microstructural analysis highlight the adverse effect of the grit blasting process. Those observations are similar to what was observed in other studies [12], [23], [30], which validates the use of our method for the characterization of coated materials. However, our methodology alone does not allow concluding on the overall impact of the grit blasting on the adhesion. Despite the obvious detrimental effects of the grit blasting on the adhesion (cracks and brittle substrate subsurface), other factors need to be accounted for. Indeed, Cizek et al. [12] reported an increase of the fatigue properties (cantilever–beam cyclic bend loading) despite the presence of embedded residual grits. This was explained by the compressive stresses in the substrate induced by the

surface preparation treatment which compensate the stress concentration induced by the increase of roughness and the embedded particles.

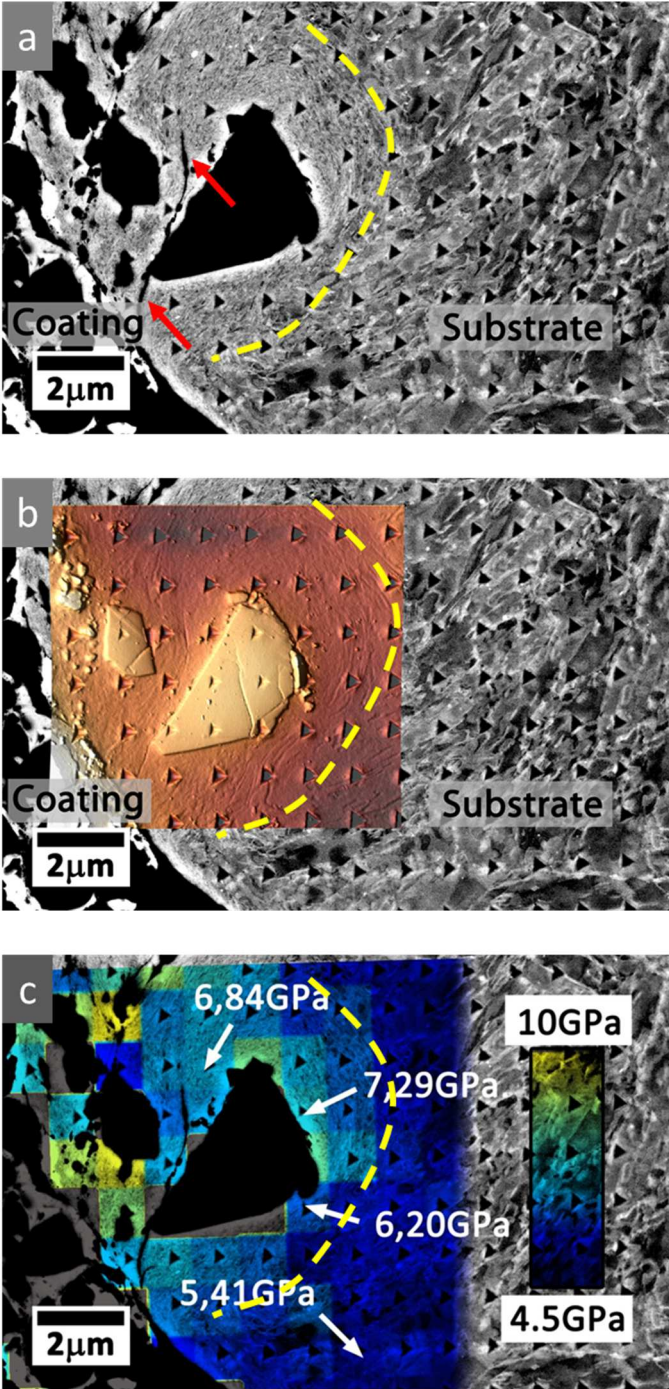


Figure 10. Nanoindentation array on an alumina particle. (a) SEM image showing the microstructure around the particle. The yellow line delimits an ultra-fine-grained structure in the vicinity of the particle. (b) Same area imaged by AFM (3D top view) that shows the deformation patterns of the surface around the particle. (c) Nanohardness map around the alumina particle. Individual hardness values are also indicated. The hardness values of the ultra-fine-grained structure are 40% higher than the bulk values.

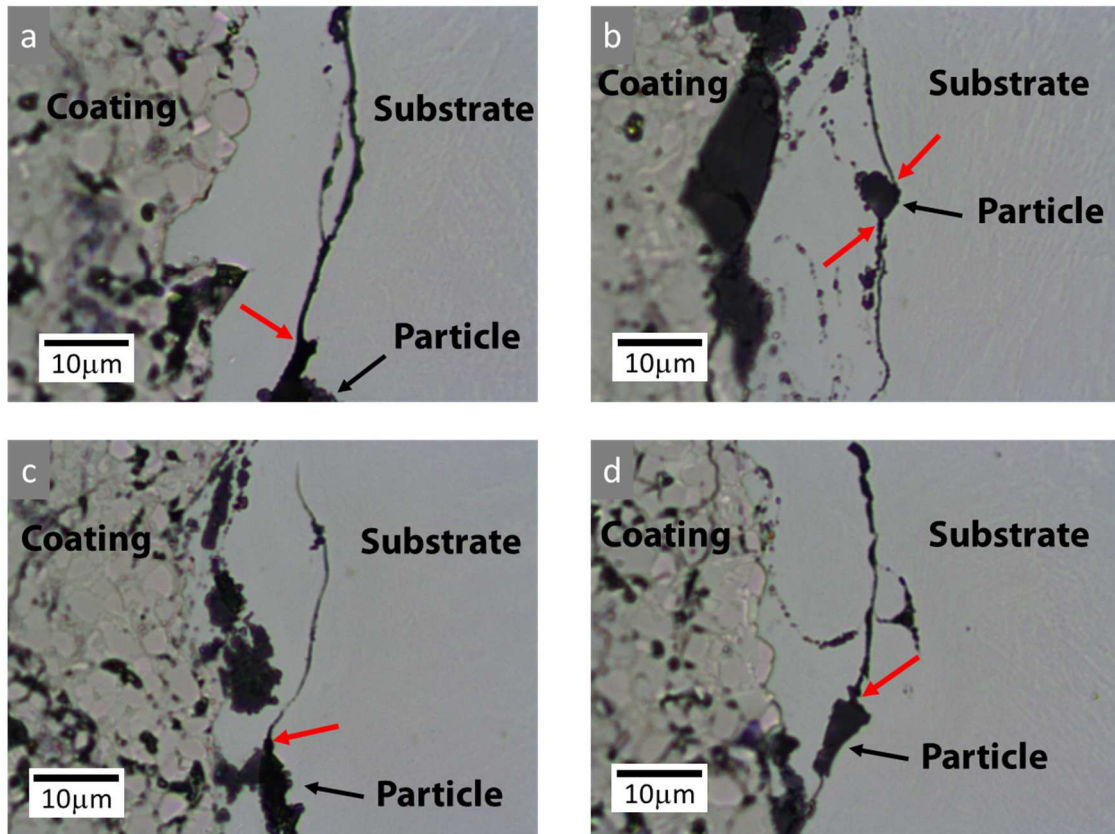


Figure 11. (a) - (d) Optical images showing different regions of the interface where cracks have nucleated from embedded alumina particles. The red arrows indicate the likely initiation site of the crack from the particle.

IV. CONCLUSION

The impact of grit blasting on a 17-4PH steel substrate coated with a cermet $\text{Cr}_3\text{C}_2\text{-NiCr}$ coating was investigated using an original method based on nanoindentation cartography coupled to microscopic observations. Despite the beneficial effect of grit blasting on adhesion through roughness modification, it was shown that the grit blasting process affects the microstructure and mechanical properties of the substrate subsurface (an average increase of more than 20% in hardness at the interface compared to the bulk values was measured). The impact of the coating deposition process on the substrate was shown to be close to zero. The potential adverse effects of the grit blasting treatment were confirmed by a local investigation of an embedded residual alumina particle. The SEM and AFM imaging, coupled to the

hardness map reconstruction from nanoindentation measurements, revealed an ultra-fine-grained microstructure associated with a further, and very local, increase of hardness (40% higher than the bulk values). Cracks nucleating from the edge of the particle were also observed suggesting that failure could preferentially occur in the layer affected by the grit blasting and not at the coating substrate interface.

Obviously, other factors could be more critical in understanding the failure of such systems. Failure in the coating or at the interface is more likely to occur. However, in a process of improving the performance of the coating, the local investigation of the impact of the substrate surface preparation is critical. Moreover, in light of the results presented in this paper, the nanoindentation cartography method couple to high resolution imaging techniques could enable to reinterpret the adhesion problems of thermal spray coating deposited on grit blasted substrate.

ACKNOWLEDGEMENT

This work was partially funded by the French Government program Investissements d'Avenir (LABEX INTERACTIFS, reference ANR-11-LABX-0017-01). We thank Anne-Marie Archambault for assistance with preparing the samples, and Dominique Eidy for helping on the SEM observations.

REFERENCES

- [1] L. Pawłowski, *The science and engineering of thermal spray coatings*. Chichester, England; Hoboken, NJ: Wiley, 2008.
- [2] V. V. Sobolev, J. M. Guilemany, J. Nutting, and S. Joshi, *High velocity oxy-fuel spraying: theory, structure-property relationships and applications*. London: Maney, 2004.
- [3] S. Kumar, G. Bae, and C. Lee, "Influence of substrate roughness on bonding mechanism in cold spray," *Surface and Coatings Technology*, vol. 304, pp. 592–605, Oct. 2016.
- [4] Y.-Y. Wang, C.-J. Li, and A. Ohmori, "Influence of substrate roughness on the bonding mechanisms of high velocity oxy-fuel sprayed coatings," *Thin Solid Films*, vol. 485, no. 1, pp. 141–147, Aug. 2005.
- [5] P. Fauchais, A. Vardelle, M. Vardelle, and M. Fukumoto, "Knowledge concerning splat formation: An invited review," *J Therm Spray Tech*, vol. 13, no. 3, pp. 337–360, Sep. 2004.

- [6] M. Baleani, M. Viceconti, and A. Toni, "The Effect of Sandblasting Treatment on Endurance Properties of Titanium Alloy Hip Prostheses," *Artificial Organs*, vol. 24, no. 4, pp. 296–299, Apr. 2000.
- [7] M. Multigner, E. Frutos, J. L. González-Carrasco, J. A. Jiménez, P. Marín, and J. Ibáñez, "Influence of the sandblasting on the subsurface microstructure of 316LVM stainless steel: Implications on the magnetic and mechanical properties," *Materials Science and Engineering: C*, vol. 29, no. 4, pp. 1357–1360, May 2009.
- [8] S. Barriuso, J. Chao, J. A. Jiménez, S. García, and J. L. González-Carrasco, "Fatigue behavior of Ti6Al4V and 316 LVM blasted with ceramic particles of interest for medical devices," *Journal of the Mechanical Behavior of Biomedical Materials*, vol. 30, pp. 30–40, Feb. 2014.
- [9] X. S. Guan, Z. F. Dong, and D. Y. Li, "Surface nanocrystallization by sandblasting and annealing for improved mechanical and tribological properties," *Nanotechnology*, vol. 16, no. 12, p. 2963, 2005.
- [10] L. Fu and D. Li, "Surface Nanocrystalline of Martensite Steel Induced by Sandblasting at High Temperature," *Adv. Eng. Mater.*, vol. 15, no. 6, pp. 476–479, Jun. 2013.
- [11] X. Tang and D. Y. Li, "Production of alloyed nanocrystalline surfaces by combined punching, sandblasting and recovery treatments," *Scripta Materialia*, vol. 58, no. 12, pp. 1090–1093, Jun. 2008.
- [12] J. Cizek, O. Kovarik, J. Siegl, K. A. Khor, and I. Dlouhy, "Influence of plasma and cold spray deposited Ti Layers on high-cycle fatigue properties of Ti6Al4V substrates," *Surface and Coatings Technology*, vol. 217, pp. 23–33, Feb. 2013.
- [13] P.-H. Gao, C.-J. Li, G.-J. Yang, Y.-G. Li, and C.-X. Li, "Influence of substrate hardness on deposition behavior of single porous WC-12Co particle in cold spraying," *Surface and Coatings Technology*, vol. 203, no. 3, pp. 384–390, Nov. 2008.
- [14] I. Horcas, R. Fernández, J. M. Gómez-Rodríguez, J. Colchero, J. Gómez-Herrero, and A. M. Baro, "WSXM: A software for scanning probe microscopy and a tool for nanotechnology," *Review of Scientific Instruments*, vol. 78, no. 1, p. 013705, Jan. 2007.
- [15] J. Woigard and J.-C. Dargenton, "An alternative method for penetration depth determination in nanoindentation measurements," *Journal of Materials Research*, vol. 12, no. 9, pp. 2455–2458, Sep. 1997.
- [16] W. C. Oliver and G. M. Pharr, "Measurement of hardness and elastic modulus by instrumented indentation: Advances in understanding and refinements to methodology," *Journal of materials research*, vol. 19, no. 1, pp. 3–20, 2004.
- [17] F.-J. Ulm, M. Vandamme, C. Bobko, J. A. Ortega, K. Tai, and C. Ortiz, "Statistical Indentation Techniques for Hydrated Nanocomposites: Concrete, Bone, and Shale," *Journal of the American Ceramic Society*, vol. 90, no. 9, pp. 2677–2692, Sep. 2007.
- [18] N. X. Randall, M. Vandamme, and F.-J. Ulm, "Nanoindentation analysis as a two-dimensional tool for mapping the mechanical properties of complex surfaces," *Journal of Materials Research*, vol. 24, no. 3, pp. 679–690, Mar. 2009.
- [19] C. Tromas, M. Arnoux, and X. Milhet, "Hardness cartography to increase the nanoindentation resolution in heterogeneous materials: Application to a Ni-based single-crystal superalloy," *Scripta Materialia*, vol. 66, no. 2, pp. 77–80, Jan. 2012.
- [20] G. C. Soltz, "The Effect of Substrate Contaminates on the Life of Epoxy Coatings Submerged in Sea Water:," Defense Technical Information Center, Fort Belvoir, VA, Mar. 1991.

- [21] A. W. Momber, *Blast cleaning technology*. Berlin: Springer Verlag, 2008.
- [22] M. Multigner, S. Ferreira-Barragáns, E. Frutos, M. Jaafar, J. Ibáñez, P. Marín, M. T. Pérez-Prado, G. González-Doncel, A. Asenjo, and J. L. González-Carrasco, "Superficial severe plastic deformation of 316 LVM stainless steel through grit blasting: Effects on its microstructure and subsurface mechanical properties," *Surface and Coatings Technology*, vol. 205, no. 7, pp. 1830–1837, Dec. 2010.
- [23] T. S. Price, P. H. Shipway, and D. G. McCartney, "Effect of cold spray deposition of a titanium coating on fatigue behavior of a titanium alloy," *J Therm Spray Tech*, vol. 15, no. 4, pp. 507–512, Dec. 2006.
- [24] M. Gross and L. Motivans, "Bimetallic MIM Medical Components - ASM International," in *Medical Device Materials*, 2004, pp. 403–407.
- [25] J. W. M. Jr, C. Kinney, K. Pytlewski, and Y. Adachi, "Microstructure and cleavage in lath martensitic steels," *Sci. Technol. Adv. Mater.*, vol. 14, no. 1, p. 014208, 2013.
- [26] X. Mao, D. Li, Z. Wang, X. Zhao, and L. Cai, "Surface nanocrystallization by mechanical punching process for improving microstructure and properties of Cu-30Ni alloy," *Transactions of Nonferrous Metals Society of China*, vol. 23, no. 6, pp. 1694–1700, Jun. 2013.
- [27] D. Tumbajoy-Spinel, S. Descartes, J.-M. Bergheau, V. Lacaille, G. Guillonéau, J. Michler, and G. Kermouche, "Assessment of mechanical property gradients after impact-based surface treatment: application to pure α -iron," *Materials Science and Engineering: A*, vol. 667, pp. 189–198, Jun. 2016.
- [28] X. Wu, N. Tao, Y. Hong, B. Xu, J. Lu, and K. Lu, "Microstructure and evolution of mechanically-induced ultrafine grain in surface layer of AL-alloy subjected to USSP," *Acta Materialia*, vol. 50, no. 8, pp. 2075–2084, May 2002.
- [29] K. Lu and J. Lu, "Nanostructured surface layer on metallic materials induced by surface mechanical attrition treatment," *Materials Science and Engineering: A*, vol. 375–377, pp. 38–45, Jul. 2004.
- [30] R. Ghelichi, D. MacDonald, S. Bagherifard, H. Jahed, M. Guagliano, and B. Jodoin, "Microstructure and fatigue behavior of cold spray coated Al5052," *Acta Materialia*, vol. 60, no. 19, pp. 6555–6561, Nov. 2012.